ISSN 0120-4211 BISTUA Vol. 5 No.1 Pag. 15 - 26

Synthesis of Zeolites and Zeotypes by Hidrothermal Transformation of Kaolinite and Metakaolinite

Ríos C.A.[1,2], Williams, C.D.[3], Maple, M.J.[3]
[1] Escuela de Geología, Universidad Industrial de Santander, Bucaramanga, Colombia
[2,3] School of Applied Sciences, University of Wolverhampton, Wolverhampton, Inglaterra
E-mail: C.A.RiosReyes@wlv.ac.uk

Recibido 23 Febrero 2007
Aceptado 02 Abril 2007

ABSTRACT
The synthesis of zeolitic materials by hydrothermal transformation of kaolinite and metakaolinite in NaOH solutions of various concentrations was investigated between 100 and 200°C, over different reaction times, using in some cases precipitated SiO2 or organic templates. Materials were obtained, including clathrasils: cancrinite (CAN), sodalite (SOD), and Linde Type A (LTA), faujasite (FAU), Na-P1 (GIS), analcime (ANA) and nepheline hydrate I (JBW) zeolites. In general, co-crystallization of CAN and SOD, likely via an unstable LTA zeolite intermediate, was observed after dissolution of kaolinite at low temperature; although the feldspathoids tend to be unstable at high temperature. LTA zeolite was synthesized after metakaolinite reaction, with minor amount of FAU zeolite, ANA and SOD. Solids were characterized by powder X-ray diffraction (XRD), Fourier transform infrared spectroscopy (FTIR), scanning electron microscopy (SEM), and thermogravimetric analysis (TGA).

KEY WORDS:
Synthesis, kaolinite, metakaolinite, cancrinite, sodalite, LTA zeolite, FTIR, SEM, XRD.

RESUMEN
La síntesis de materiales zeolíticos a partir de la transformación hidrotermal de caolinita y metacaolinita en soluciones de NAOH se investigo entre 100 y 200°C, durante diferentes tiempos de reacción, usando en algunos casos SiO_2 precipitada o templantes orgánicos. Los materials obtenidos incluyen cancrinita (**CAN**), sodalita (**SOD**), y Linde Type A (**LTA**), faujasita (**FAU**), Na-P1 (**GIS**), analcima (**ANA**) y nefelina hydratada I (**JBW**).En general, se observo la co-cristalización de **CAN** y **SOD**, posiblemente vía zeolita **LTA**, una fase metastable intermedia, a partir de la disolución de la caolinita. Zeolita **LTA** fue sintetizada a partir de la reacción de la metacaolinita, con menor cantidad de zeolita **FAU**, **ANA** y **SOD**. Los sólidos fueron caracterizados por difracción de rayos X, espectroscopia infrarroja transformada de Fourier, microscopio electrónica de barrido, y análisis termogravimétrico.

PALABRAS CLAVES
Síntesis, caolinita, metacaolinita, cancrinita, sodalita, zeolita LTA

INTRODUCTION

Zeolites are crystalline, microporous, hydrated aluminosilicates of alkaline or alkaline earth metals. The frameworks are composed of $[SiO_4]^{4-}$ and $[AlO_4]^{5-}$ tetrahedra, which corner-share to form different open structures. The negative charge on the lattice is neutralised by the positive charge of cations located within the material's pores. In the basic zeolites these are usually univalent and bivalent metals or a combination. The metal cations may be replaced by acidic protons *via* ion-exchange to ammonium and subsequent calcination. By reason of electrostatic forces it is not possible to make an Al-O-Al bond. They are made up of «T-atoms» which are tetrahedrally bonded to each other with oxygen bridges. Other "T-atoms" such as P, Ga, Ge, B, Be, etc. can exist in the framework as well.

The synthesis of zeolites in forms suitable for industrial applications is of great importance. The first natural zeolite was discovered by Cronstedt in 1756, and the first synthesis was attempted by St. Claire-Deville in 1862. Barrer's pioneering work in 1940s demonstrated that a wide range of zeolites could be synthesized from aluminosilicate gels. The discovery that quaternary ammonium salts could act as structure directing agents (SDAs), sometimes called "templates", has resulted in the preparation of nearly 100 different silicate frameworks (International Zeolite Association, www.iza-structure.org). The mode of action of the SDA has been extensively investigated by Davies and Zones and this has led to some empirical rules, if not the absolute ability to design new solids (Lobo et al, 1995). Use of fluoride as a mineraliser in zeolite synthesis was developed by Flanigen in the 1970s and has resulted in zeolites being prepared with fewer defect sites and higher silica contents.

At present, synthetic zeolites are used commercially more often than natural zeolites due to the purity of crystalline products and the uniformity of particle sizes (Breck, 1974). However, the preparation of synthetic zeolites from chemical sources of silica and alumina is expensive. Such costs may be reduced by the use of clay minerals, volcanic glasses (perlite and pumice), rice husks, diatoms, fly ash or paper sludge ash as starting materials. Zeolite synthesis has been also developed by the transformation of one zeolite type into other zeotypes.

Previous work has shown that kaolinite is not stable under highly alkaline conditions and different zeolitic materials can form, and that kaolinite is usually used after calcination to obtain a more reactive phase (metakaolinite). After dehydration (endothermic dehydroxylation), kaolinite is transformed into amorphous metakaolinite. Raw kaolinite and metakaolinite have been used as the Al and Si sources for synthesis of zeolites Linde Type A, X, Y, P, 4A, Na-A, KI, cancrinite, sodalite, hydroxysodalite, faujasite, phillipsite, chabazite and several other types of zeolites (e.g., Dudzik and Kowalak, 1974; Buhl, 1991; Rees & Chandrasekhar, 1993; Alberti et al., 1994; Buhl & Loens, 1996; Gualtieri et al., 1997; Akolekar et al., 1997; Bauer & Berger, 1998; Bauer et al., 1998; Sanhueza et al., 1999; Barnes et al. 1999a, 1999b, 1999c; Buhl et al., 2000a, 2000b; Park et al., 2000; Chorover et al., 2003; Zhao et al., 2004; Mon, et al., 2005; Covarrubias et al., 2006).

In this paper we investigate the hydrothermal reaction of kaolinite or metakaolinite in alkaline solutions. Moreover, we adjust the SiO_2/Al_2O_3 ratio at selected compositions with precipitated or fly ash and introduce organic structure directing agents. In this way we explore the influence of reaction time, NaOH and Al concentrations in the hydrothermal treatments.

MATERIALS AND METHODS

Materials were synthesized hydrothermally by treating kaolinite (Supreme Powder, ECC International, UK) or metakaolinite with solutions of sodium hydroxide (99 %, Aldrich). Kaolinite (composition 46.44 % SiO_2, 38.80 % Al_2O_3, 0.03 % TiO_2, 0.52 % Fe_2O_3, 0.08 % MgO, 0.33 % Na_2O and 0.69 % K_2O) was used without further purification. Metakaolinite was

prepared by calcining kaolinite at either 600, 950 or 1000 °C in air for 2 hours. All solid starting materials were first ground and particles of less than 75 μm selected by sieving, before gels were prepared by mixing with aqueous NaOH. The resulting mixtures were transferred to either 65 cm^3 polytetrafluoroethylene (PTFE)-bottles (Cowie Technology) or 20 cm^3 PTFE-lined stainless steel autoclaves and heated under static conditions at 100 or 200°C for different reaction times. On removal from the oven they were quenched in cold water and the product recovered by vacuum filtration, washed with distilled water and dried at 80°C overnight.

To examine the effect of modifying the SiO_2/ Al_2O_3 ratio experiments were preformed in which this was adjusted by the addition SiO_2, either as precipitated silica (98 %, BDH). Furthermore, in selected preparations, tetrapropylammonium bromide (98 %, Aldrich) or triethanolamine, (AnalaR, BDH) were added as structure directing agents (SDAs). Further details of the gel compositions and synthesis conditions are given in Table 1.

All solids were identified by powder X-ray diffraction (XRD), performed on a Philips PW1710 diffractometer equipped with Cu-Kα radiation and theta compensating divergence slits. Data were collected in 45 min over the 2θ range 3-50°, with a step size of 0.02° with phase identification being made by searching the ICDD powder diffraction file database. Fourier transform infrared (FT-IR) spectra were recorded in the range 400-4000 cm^{-1} on a Mattson Genesis II system. Crystal morphology was examined by a Zeiss EVO 50 scanning electron microscope on gold-coated samples. Thermogravimetry was performed on a Mettler Toledo TG50 thermobalance in the temperature range of 25-900°C (for kaolinite) and 25-700°C (for zeolitic products), with a heating rate of 10°C min^{-1} under flowing air. Chemical analysis was carried out with a Spectro XEPOS X-ray fluorescence (XRF) spectrometer on powders mounted behind prolene film.

RESULTS

X-ray diffraction

XRD patterns of unheated and activated (600, 950 and 1000°C) kaolinite are shown in Figure 1. Kaolinite is identified by its characteristic X-ray diffraction peaks at 12.34° and 24.64° 2? as has been reported in previous studies (Zhao et al., 2004). After thermal treatment, the XRD patterns exhibit a significant change in comparison to the pattern of untreated kaolinite, which is characterized by the disappearance of the diffraction peaks of kaolinite, accompanied by the appearance of an amorphous aluminosilicate (see the broad hump at 2? = 13-33°), which persists between 600 and 950°C, with relicts of the original kaolinite. However, this amorphous material contains mullite as the main crystalline phase at 1000°C. Therefore, the activation of kaolinite produces structural changes of this mineral, promoting its reactivity to synthesize zeolitic materials.

The X-diffraction patterns of unreacted and reacted kaolinite treated with alkaline solutions are presented in Figure 2. The most distinct changes in the XRD patterns are the reduction in intensity of the kaolinite peaks and the appearance of new crystalline phases. The hydrothermal treatment of kaolinite in low NaOH solutions resulted in the crystallization of **CAN** and **SOD**, along with metastable **LTA** zeolite (Figures 2-1a and 2-1b). When precipitated SiO_2 was used a high Si/Al ratio **LTA**, **FAU** and **GIS** zeolites with minor amount of **CAN** and **SOD** was formed (Figures 2-2a and 2-2b), which is reflected in strong peaks for these zeolites and relatively weak peaks for the feldspathoids, compared with what is observed in Figures 2-1a and 2-1b. No interesting changes were observed using tetrapropylammonium bromide (Figures 3-1a and 3-1b). In general, at low reaction times (Figures 2-1a, 2-2a and 2-3a) the raw kaolinite is dominant respect to the as-synthesized products, which display low intensity peaks compared with those in Figures 2-1b, 2-2b and 2-3c, respectively. Higher NaOH solutions produced a faster dissolution of the original

kaolinite accompanied by more crystalline zeolitic materials. The relative height of the diffraction peaks of **CAN** and **SOD**, as well as **LTA** zeolite increased as shown in Figures 2-4a and 2-4b (compared with Figures 2-1a and 2-1b). A reaction at higher temperature promoted an increase in intensity of the **LTA** zeolite, as well as the appearance of **JBW**, **ANA** and **FAU** zeolites (Figures 2-5a and 2-5b). When triethanolamine was used **CAN** and **SOD** were the main dominant crystalline phases at low reaction time (Figure 2-6a), whereas **LTA, ANA** and **FAU** zeolites (Figure 2-6b) crystallized with weak diffraction peaks for **CAN** and **SOD** at high reaction time.

In Figure 3 the XRD patterns of metakaolinite and the resulting as-synthesized products after its hydrothermal reaction with alkaline solutions are illustrated. The most important change observed in the XRD patterns is the appearance of the characteristic peaks of **LTA**, **FAU** and **ANA** zeolites. The as-synthesized **LTA** zeolite has several common peaks located at 7.14°, 10.10°, 12.38°, 16.20°, 21.58°, 23.92°, 27.00°, 29.82° and 34.08° 2? on its XRD pattern (Figures 3-7a and 3-7b). When precipitated SiO_2 was used, the as-synthesized product show intensity peaks of **LTA** zeolite at low reaction time (Figure 3-8a), which however disappear with reaction time to produce an amorphous aluminosilicate material (Figure 3-8b). Using tetrapropylammonium bromide a reduction in the intensity of the peaks of **LTA** zeolite was observed (Figures 3-9a and 3-9b). However, at higher NaOH concentration and temperature, using precipitated SiO_2, a mixture of **LTA**, **FAU** and **ANA** zeolites were obtained (Figures 3-10a and 3-10b).

FTIR spectroscopy

The FTIR spectra of the original kaolinite and as-synthesized products obtained after its hydrothermal treatment with alkaline solutions are shown in Figure 4a, and the assignment of their spectral frequencies are given in Table 2. We recognize the characteristic OH-stretching vibrations of kaolinite at 3687 cm^{-1} (surface OH stretching) and 3619 cm^{-1} (inner OH stretching), as well as the peaks at 1115, 1030, 1007, 937 (surface OH bending), 912 (inner OH bending), 800, 792 and 751 cm^{-1}, which disappeared after hydrothermal reaction. However, the peaks at 689, 647 and 535 cm^{-1} were shifted to higher frequencies, and the vibration bands at 466 and 430 cm^{-1} were shifted to lower frequencies. Coincident with the disappearance of kaolinite, characteristic zeolite bands appeared on the spectra, including the asymmetric Al-O stretch located in the region of 950-1250 cm^{-1}, and their symmetric Al-O stretch located in the region of 660-770 cm^{-1}. The bands in the region of 500-650 cm^{-1} are related to the presence of the double rings (D4R and D6R) in the framework structures of the zeolitic materials. The bands in the region of 420-500 cm^{-1} are related to internal tetrahedron vibrations of Si-O and Al-O of the synthetic zeolites. The bands in the region of 400-420 cm^{-1} are related to the pore opening or motion of the tetrahedra rings, which form the pore opening of zeolites (Breck, 1974).

Figure 4b illustrates the FTIR spectra of the unreacted and reacted metakaolinite in alkaline solutions, whereas the assignment of their spectral frequencies is presented in Table 2. The transformation of kaolinite to metakaolinite can be observed, by comparing Figures 5a and 5b, showing the loss of Al-OH bands (937 and 912 cm^{-1}), changes in the Si-O stretching bands, and the disappearance of Al-O-Si bands at 788 and 751 cm^{-1}. These changes are similar to those reported in other studies (Akolekar et al., 1997; Zhao et al., 2004; Covarrubias et al., 2006). The characteristic bands observed in the metakaolinite were 1043, 796, 562 and 422 cm^{-1}. Three broad bands are centered at 1043, 796 and 422 cm^{-1}. A significant shift of the Si-O vibration bands at 1030 and 1007 cm^{-1} in kaolinite to a higher frequency band at 1043 cm^{-1} in metakaolinite was observed, which has been assigned to amorphous SiO_2 as reported by Sinha et al. (1995) and Valcke et al. (1997). The band located at 796 cm^{-1} was not observed in the zeolitic products, whereas the band at 1043 cm^{-1} was shifted to the bands at 970, 974, 964 and 972 cm^{-1}. The low intensity band at 562 cm^{-1} was shifted to low frequency bands (538, 527, 532 and 527 cm^{-1}).

The band at 455 cm^{-1} is close to the band at 456 cm^{-1} (bending vibrations of the TO4) of **FAU** zeolite. The bands at 557, 684 and 970 cm^{-1} are close to the bands at 560, 686 and 971 cm^{-1}, which corresponds to the 6-membered double-ring vibration, to the symmetric stretching and to the asymmetric stretching, respectively, of **FAU** zeolite. The band at 557 cm^{-1} could represent the beginning of the crystallization of a zeolite with double rings (Alkan et al., 2005). The bands at 463 and 671 or 672 cm^{-1} are close to the bands at 462 and 668 cm^{-1} assigned to the internal linkage vibrations of the TO4 (T = Si or Al) tetrahedra and to the asymmetric stretching, respectively, of **LTA** zeolite. However, the band at 463 cm^{-1} is close to the band at 461 cm^{-1}, which indicates the presence of hydroxysodalite. The band at 600 cm^{-1} corresponds to the double-ring vibration of **GIS** zeolite, whereas the bands at 671 or 672 cm^{-1} are close to the band at 670 cm^{-1} (symmetric stretching) of this zeolite. The band at 621 cm^{-1} is close to the band at 618 cm^{-1} assigned to the 6-membered double-ring vibration of **CAN**. The band at 663 cm^{-1} (corresponds to the symmetric stretching) is close to the band at 660 cm^{-1}, which was also observed, of this zeolite-like material.

Scanning electron microscopy

SEM micrographs (Figures 5 and 6) of the as-synthesized products after hydrothermal treatment of kaolinite and metakaolinite show a marked change in the morphology of the starting materials. Kaolinite can be recognized by its platy morphology and hexagonal outlines (Figure 5a). A predominantly lephispheric morphology is typically observed in the zeolitic products obtained after hydrothermal reaction of kaolinite in 1.33M NaOH solutions at 100°C for 120 hours with spheroidal «ball of yarn» morphologies for **SOD** and rod-shaped structures for **CAN** (Figure 5b). **LTA** zeolite can be identified by its characteristic cubic morphology (Figure 5c); it probably formed before **CAN** and **SOD**, as shown by the occurrence of crystals of these feldspathoids growing at the surface of **LTA** zeolite. Figure 5d illustrates s pheroidal aggregates of cubic crystals of **LTA** zeolite, showing penetrating twinning, which were obtained at 1.33M NaOH + precipitated SiO_2 at 100°C for 96 hours. In some cases, an intergrowth of crystals of **LTA** and **FAU** zeolites are observed in these spheroidal morphologies (Figure 5e). Characteristic long prismatic lath-like crystals of **JBW** zeolite (Figure 5f) were produced after hydrothermal treatment of kaolinite at 3.99M NaOH at 200°C for 168 hours. On the other hand, the hydrothermal treatment of metakaolinite reflects a common occurrence of cubic crystals of **LTA** zeolite. Lephispheric morphologies corresponding to **CAN** and **SOD** grow at the surface of cubic crystals of **LTA** zeolite, which sometimes display interpenetrating twinning, (Figures 6a and 6b), at 1.33M NaOH solutions at 100°C for 52 hours. Some deformed pseudohexagonal platelets of the original kaolinite still remain after its activation. When precipitated SiO_2 was added to the reaction gel, amorphous spheroidal morphologies, from which aggregates of very small cubic **LTA** zeolite crystals are growing (Figure 6c) were obtained at 1.33M + precipitated SiO_2 at 100°C for 96 hours, whereas massive to clusters of radiating needlelike crystals of **SOD** (Figure 6d) crystallized at higher NaOH concentration and temperature.

Thermogravimetric Analysis (TGA)

TG/DTG curves of starting kaolinite and as-synthesized products are shown in Figure 7. The characteristic DTG peaks and weight loss percentages of zeolitic products and starting materials are presented in Table 1. The DTG curve of the kaolinite (Figure 7a) displays a strong peak at 517°C, which is due to dehydroxylation of kaolinite within the 450-600°C temperature range resulting in a weight loss of 15.34% and formation of metakaolinite. The peak on the DTG curve at approximately 980°C is an evidence of breakdown of the metakaolinite structure and the formation of mullite. The as-synthesized products show three or four dehydration steps. The position of these DTG peaks and the number of dehydration steps has been attributed to the different compensating cation-water binding energies as well as to the different energy associated with the diffusion of the desorbed water through the porous structure of the zeolitic materials; their weight loss percentages reflects the water loss from the zeolite structure, and the

amount of desorbed water is related with the number of compensation cations in the framework of the zeolite (Covarrubias et al., 2006). Figures 7b and 7c illustrate the DTG curves corresponding to zeolitic materials synthesized from kaolinite and metakaolinite, respectively. The peaks observed between 39 and 52°C correspond to surface water in zeolitic materials; the peaks observed between 100 and 162°C indicate zeolitic water, although in some cases in this range of temperature up to two peaks occur, which can be explained by the heterogeneous nature of the as-synthesized products. There are also some peaks in the range of temperature 216-257°C. The peaks at 141, 223 and 237°C are related to the vaporizing of the organic template. However, sometimes these peaks are broad, which indicate that water and the organic template are coming out from the zeolite. A broad peak around 500°C is indicating the burning of the organic template. The as-synthesized products obtained after hydrothermal transformation of kaolinite in solutions of 1.33M NaOH + precipitated SiO_2 at 100°C for 96 hours display the highest weight loss (17.88%), which indicates that these zeolitic products have a higher amount of water. On the other hand, zeolitic products obtained after hydrothermal transformation of kaolinite in alkaline solutions show a decrease in weight loss with increasing the NaOH concentration. The lowest weight loss (8.10%) was obtained for zeolitic materials formed after reaction of kaolinite in solutions of 3.99M NaOH + triethanolamine at 200°C for 48 hours. The synthetic zeolitic products obtained after hydrothermal transformation of metakaolinite in solutions of 1.33M NaOH at 100°C for 52 hours shows the highest weight loss (19.48%).

DISCUSSION

Based on this study, the kaolinite ($Al_2Si_2O_5(OH)_4$) experienced chemical transformation by dehydroxylation between 450 and 600°C, which results in the formation of metakaolinite ($Al_2Si_2O_7$). The decomposition of metakaolinite at a temperature between 980 and 1000°C produces an amorphous material from which mullite crystallized, that is consistent with the results obtained by XRD.

There is evidence that **LTA**, **FAU**, **GIS** and **JBW** zeolites and feldspathoids (**CAN**, **SOD** and **ANA**) are present in the reaction products after hydrothermal treatment of raw materials in alkaline solutions. There were two major chemical processes involved in the reaction between kaolinite (or metakaolinite) and alkaline solutions: dissolution of kaolinite (or metakaolinite) followed by formation of zeolitc materials. The structural similarity between zeolites and feldspathoids explain why them can coexist in the as-synthesized products and the dominant crystalline phase depends on the conditions of formation.

The dissolution of kaolinite is favored at high NaOH concentrations, which is probably the reason why more kaolinite converted to zeolitic materials in alkaline solutions of 3.99M NaOH than solutions of lower concentration of NaOH. The main crystalline phases obtained at low NaOH solutions and temperatures were **CAN**, **SOD** and **LTA** zeolite. **FAU** and **GIS** zeolites also crystallized at high SiO_2/Al_2O_3 ratio solutions. On the other hand, at high NaOH solutions and temperatures, similar phases crystallized, except by the formation of **JBW** and **ANA** A high crystallinity **LT**A zeolite was obtained. We suppose that **CAN** appeared more stable than **SOD**, and would be the final product, whereas amorphous material, **LTA** zeolite and **SOD** would be the transition phases at low NaOH concentrations and temperature, and that during the hydrothermal transformation of kaolinite an initial formation of **SOD** occurred with subsequent transformation to **CAN** as has been reported in other studies (e.g., Barnes et al., 1999a; Choi et al., 2005b). However, different zeolites crystallized at high NaOH concentrations and temperature, with minor amount of **CAN** or **SOD**.

LTA zeolite was the most important zeolitic material that crystallized after hydrothermal treatment of activated metakaolinite. When precipitated SiO_2 was used at low NaOH concentrations and temperature, an amorphous aluminosilicate phases was obtained, but when this silica source was used at high NaOH concentrations and temperature, high crystallinity

phases such as **LTA** and **FAU**, along with **ANA**, were obtained. The use of organic templates produced **LTA** zeolite with a low crystallinity compared with that obtained without using it.

The production of microporous materials by the reaction of kaolinite or metakaolinite with NaOH solutions at 100°C or 200°C and different reaction times does not represent a new synthesis, but provides valuable scientific knowledge on their transformation on the nucleation and growth of aluminosilicates, with dissolution dominating initially and precipitation dominating in the later stages.

Only **LTA** and **JBW** zeolites were produced as nearly pure crystalline phases from hydrothermal reaction of metakaolinite and kaolinite, respectively.

For a future research we are going to evaluate the efficiency of such zeolitic materials in selective cation exchange as a potential remediation alternative for purification of waste waters, analyzing the incorporation and diffusion of contaminant cations (e.g., Cs or Sr) in their structures , similar to what have been reported in previous studies (e.g., Serne et al., 1998; Flury et al., 2002; Chorover et al., 2003; Liu et al., 2003; Mashal, 2003; Zhao et al., 2004; Mon et al., 2005; Choi et al., 2005a, 2005b).

Different hybrid organic–inorganic zeolitic materials could be synthesized containing into their frameworks organic groups. However, the introduction of organic linkers requires very long synthesis times because the hydrolysis and polycondensation of organic groups covalently bonded to inorganic matrix retard the crystallization process. The zeolite framework is a very important parameter to introduce higher or lower amount of organic groups inside of its networks.

ACKNOWLEDGMENTS

We are grateful to the Programme Alban, the European Union Programme of High Level Scholarships for Latin America, scholarship No. E05D060429CO, and the Universidad Industrial de Santander (a remunerated commission) for funding C. Rios. Special thanks to School of Applied Sciences at University of Wolverhampton for allowing us the use of the research facilities. The authors acknowledge to Dr. Catherine Duke for her critical and insightful reading of the manuscript. We also thank Dave Townrow and Mrs Barbara Hodson for assistance with the adquisition of XRF and SEM data, respectively. The authors are most grateful to the above-named people and institutions for support

Table 1

Synthesis conditions for hydrothermal treatment of kaolinite and metakaolinite and DTG peaks and weights loss for starting materials and zeolitic products.

Batch composition of the reaction gel	[NaOH] (M)	SDA	Temperature (°C)	Time (hour)	As-synthesized products	DTG peaks (°C) T1	T2	T3	T4	T5	Weight loss (%)
Kaolinite						45	517				15.34
$Na_2O:Al_2O_3:2SiO_2:86.4H_2O$	1.33		100	6	1a c, s, A						
				120	1b c, s, A	46	100	216	483		14.57
$Na_2O:Al_2O_3:2SiO_2:86.6H_2O^s$	1.33		100	24	2a c, s, A, F, P						
				96	2b c, s, A, F, P	46	107	162	264	483	17.88
$Na_2O:Al_2O_3:2SiO_2:0.5(CH_3)_4NBr:86.3H_2O$	1.33	$(CH_3CH_2CH_2)_4NBr$	100	6	3a c, s, A						
				120	3b c, s, A	39	128	223	497		17.87
$3Na_2O:Al_2O_3:2SiO_2:88.5H_2O$	3.99		100	6	4a c, s, A, P						
				120	4b c, s, A, P	46	59	134	155	216	13.02
$3Na_2O:Al_2O_3:2SiO_2:88H_2O$	3.99		200	24	5a c, s, a, A, F, N						
				168	5b c, s, a, A, F, N	52	107	230			9.17
$Na_2O:Al_2O_3:2SiO_2:0.5(CH_2CH_2OH)_3N:88.3H_2O$	3.99	$CH_2CH_2OH)_3N$	200	6	6a c,s						
				48	6b c, s, a, A, F	237					8.11
Metakaolinite											
$Na_2O:Al_2O_3:2SiO_2:90.3H_2O^*$	1.33		100	22	7a A						
				52	7b A	39	134				19.48
$Na_2O:Al_2O_3:2SiO_2:84.5H_2O^{*,s}$	1.33		100	24	8a A						
				96	8b	46	107	155	257		15.82
$Na_2O:Al_2O_3:2SiO_2:0.5(CH_3)_4NBr:84.2H_2O^{**}$	1.33	$(CH_3CH_2CH_2)_4NBr$	100	22	9a A						
				52	9b A	46	141				18.85
$Na_2O:Al_2O_3:2SiO_2:85.8H_2O^{*,s}$	3.99		200	6	10a F, a, c, s						
				48	10b F, a, c, s	39	107	121	688		18.65

** activated kaolinite at 600 °C; ** activated kaolinite at 950 °C; s precipitated SiO_2 ; $(CH_3CH_2CH_2)_4NBr$, tetrapropylammonium bromide; $CH_2CH_2OH_3N$, triethanolamine. c, **CAN** ; s, **SOD** ; a, **ANA** ; A, **LTA** zeolite; F, **FAU** zeolite; P, **GIS** zeolite; N, **JBW** zeolite.*

Table 2
Fourier transformed infrared assignments of raw materials and as-synthesized products.

Assignment	Raw	Zeolitic products											Raw	Zeolitic products							
(cm^{-1})	Kaolinite	1a	1b	2a	2b	3a	3b	4a	4b	5a	5b	6a	6b	Metakaolinite	7a	7b	8a	8b	9a	9b	10a	10b
Asymmetric T-O stretching vibrations	1115	1117		1116		1115					1101	1114	1117									
				1004																		
	1030	1031		1030										1043								
	1007	1007		1007		999				1006												
						984											980				984	
					975					966					976	970		974	972			972
			959				960	964	959		955	961	957							964		
	937	949		942																		
	912	918		915		922																
								888														
	800			800																		
	792	797		793		795								796								
Symmetric T-O stretching vibrations										768	762	768	762									
	751			756																		
			720		720			724														
	689	701	699	697	697	698	698	702	699								683	684			689	681
		665			662	663	660	662	660	675	671	676	673		677	672			675	663		
	647																					
4- or 6-membered double rings					621					627	623	628	623									
			607							606	600	607	603									
										561	557	563	558	562								
	535	540	536	537	533	540	536	539	536						544	538	542	527		532		527
Bending vibrations of T-O	466	469	455	468	463	463	455	455	455	457	455	456	456									
	430	431		428																		
	423		422	422	422	424	420	423	422					422	427	419	422		417		422	
	416			413						407	403	405	406					409		413		411

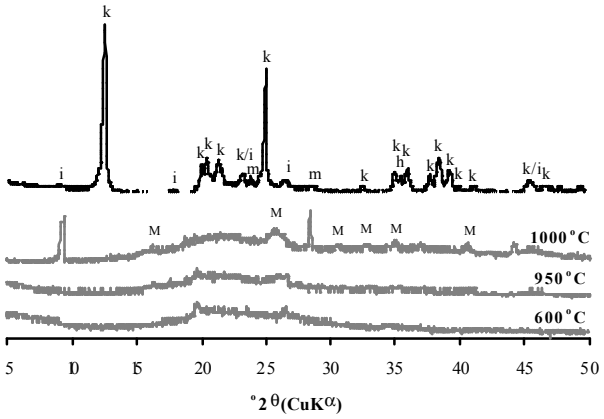

Figure 1. X-diffraction patterns of uncalcined and calcined kaolinite at different temperatures. i, illite; k, kaolinite; m, muscovite; h, halloysite; M, mullite.

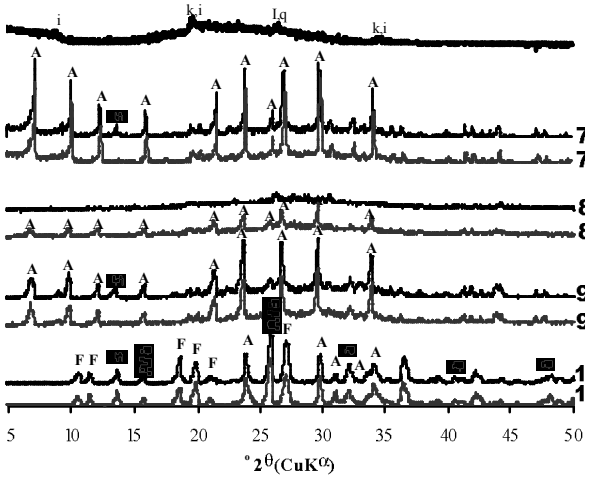

Figure 3. X-ray diffraction patterns of unreacted (upper part) and reacted metakaolinite treated with alkaline solutions. The numbers indicating XRD patterns correspond to the as-synthesized products column in Table 1. i, illite; q, quartz; A, **LTA** zeolite; F, **FAU** zeolite; a, **ANA**; c, **CAN**; s, **SOD**.

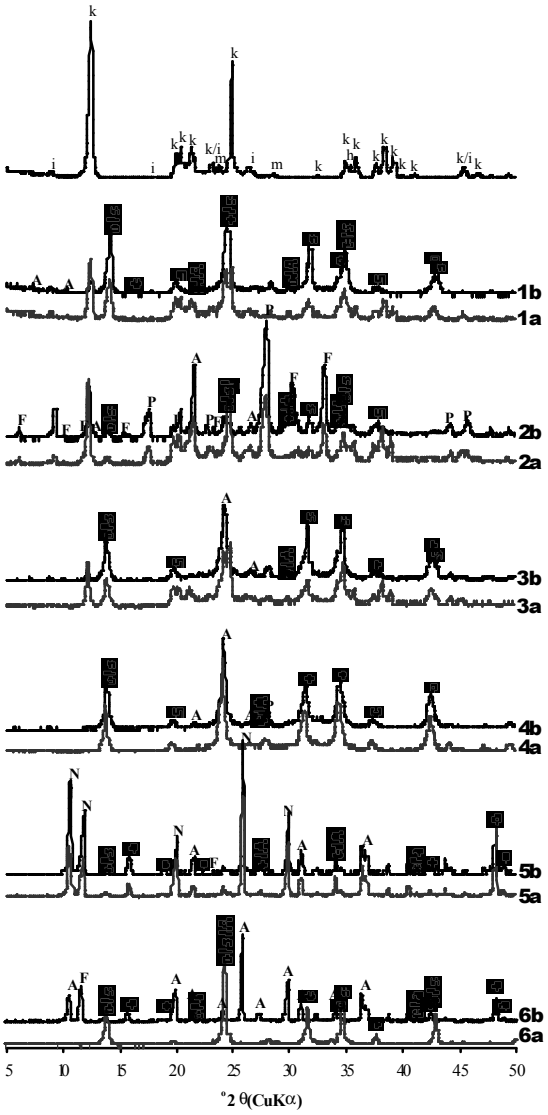

Figure 2. X-diffraction patterns of unreacted (upper part) and reacted kaolinite treated with alkaline solutions. The numbers indicating XRD patterns correspond to the as-synthesized products column in Table 1. k, kaolinite; i, illite; m, muscovite; h, halloysite; c, **CAN**; s, **SOD**; A, **LTA** zeolite; F, **FAU** zeolite; P, **GIS** zeolite; N, **JBW** zeolite.

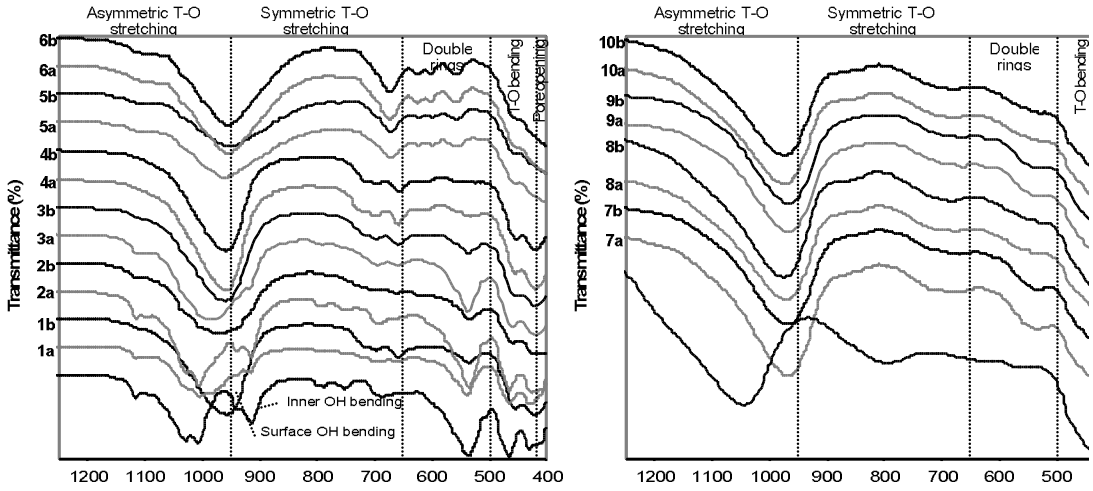

Figure 4. FTIR spectra of unreacted and reacted (a) kaolinite and (b) metakaolinite treated with alkaline The numbers indicating FTIR spectra correspond to the as-synthesized products column in Table 1.

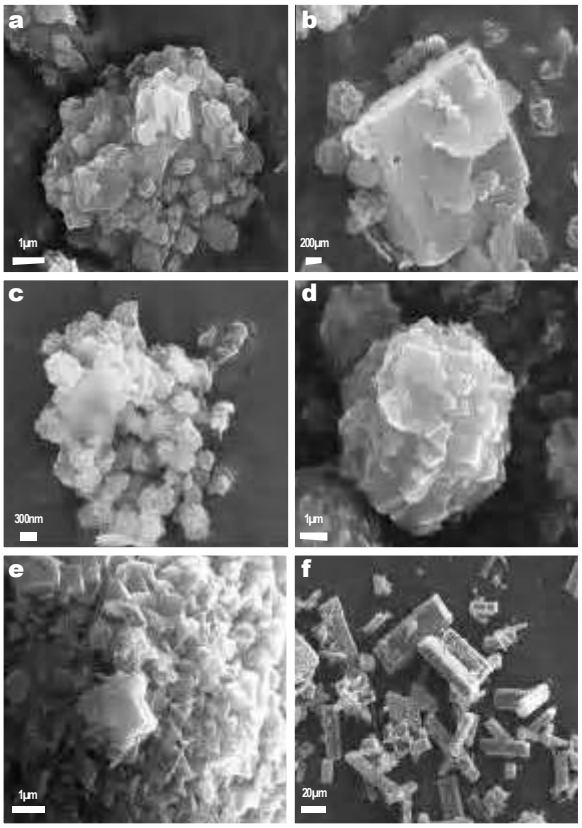

Figure 5. Scanning electron microscopy images of (a) hexagonal platy crystals of unreacted kaolinite, (b) crystals of **CAN** and **SOD** growing at the surface of a cubic crystal of **LTA** zeolite, (c) lephispheric morphology of aggregates of **CAN** and **SOD** and relict kaolinite, (d) spheroidal aggregates of cubic crystals of **LTA** zeolite, showing penetrating twinning, (e) detail of a lephispheric morphology showing an intergrowth of crystals of **LTA** and **FAU** zeolites, (f) long prismatic lath-like crystals of **JBW**.

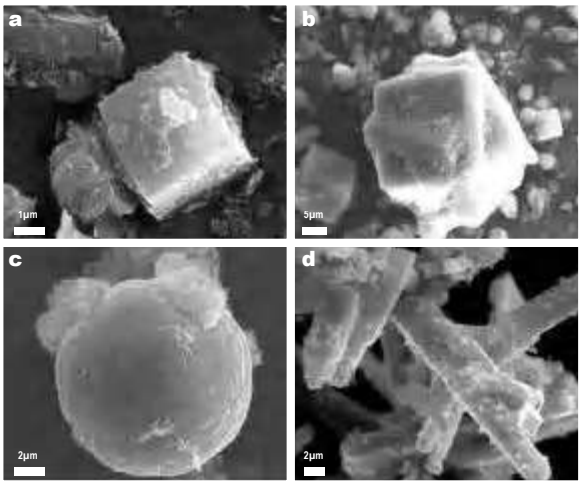

Figure 6. Scanning electron microscopy images of (a) lephispheric morphology of **CAN** or **SOD** associated to a cubic crystal of **LTA** zeolite, with crystals of the feldspathoids growing at the surface of **LTA** zeolite; observe some deformed pseudohexagonal platelets of the original kaolinite, (b) cubic **LTA** zeolite, displaying interpenetrating twinning, (c) amorphous spheroidal morphology from which aggregates of cubic **LTA** zeolite crystals are growing, (d) massive to clusters of radiating needlelike crystals of **SOD**.

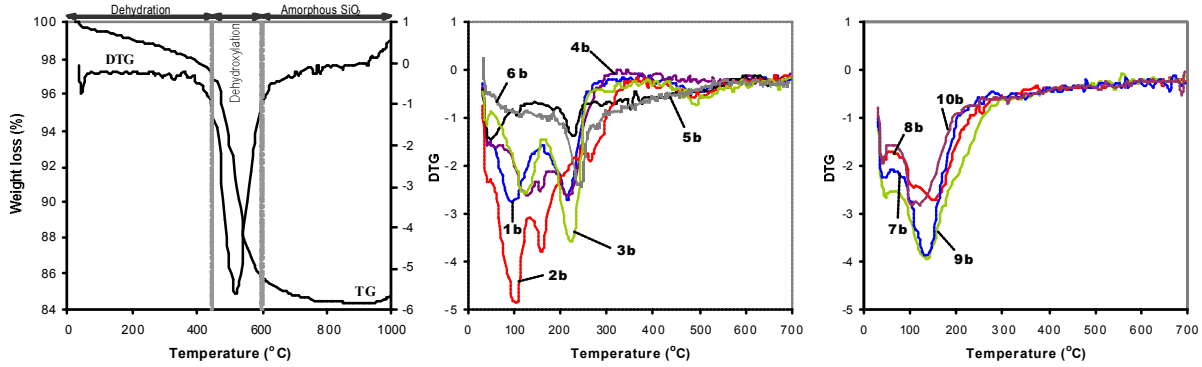

Figure 7. (a) TG/DTG curves from 25 to 1000°C of raw kaolinite. (b) and (c) DTG curves from 25 to 700°C of zeolitic phases obtained after hydrothermal treatment of kaolinite and metakaolinite, respectively, with alkaline solutions. The numbers indicating DTG curves correspond to the as-synthesized products column in Table 1.

REFERENCES

Akolekar D, Chaffee A, Howe, R (1997) The transformation of kaolin to low-silica X zeolite. Zeolites. Vol. 19, No. 5: 359-365.

Alberti A, Colella C, Oggiano G, Pansini, M, Vezzalini, G (1994) Zeolite production from waste kaolin containing materiales. Materiales Engineering (Modena, Italy). Vol. 5: 145-158.

Alkan, M, Hopa, C, Yilmaz, Z, Güler, H (2005) The effect of alkali concentration and solid/liquid ratio on the hydrothermal synthesis of zeolite NaA from natural kaolinite. Microporous Mesoporous Materials. Vol. 86: 176-184.

Aronne, A, Esposito, S, Ferone, C, Pansini, M, Pernice, P (2002) FTIR study of the thermal transformation of barium-exchanged zeolite A to celsian. Journal of Materials Chemistry. Vol. 12: 3039-3045.

Barnes MC, Addai-Mensah J, Gerson AR (1999a) The mechanism of the sodalite-to-cancrinite phase transformation in synthetic spent Bayer liquor. Microporous Mesoporous Materials. Vol. 31: 287-302.

Barnes, MC, Addai-Mensah, J, Gerson, AR (1999b) A methodology for quantifying sodalite and cancrinite phase mixtures and the kinetics of the sodalite to cancrinite phase transformation. Microporous Mesoporous Materials. Vol. 31: 303-319.

Barnes, MC, Addai-Mensah, J, Gerson, AR (1999c) The solubility of sodalite and cancrinite in synthetic spent Bayer liquor. Colloids and Surfaces A, Physicochemical and Engineering Aspects. Vol. 157: 106-116.

Barrer, RM (1978) Zeolites and Clay Minerals as Sorbents and Molecular Sieves. Academic Press, London.

Bauer A, Berger G (1998) Kaolinite and smectite dissolution rate in high molar KOH solutions at 35° and 80°C. Applied Geochemistry. Vol. 13: 905-916.

Bauer A, Velde B, Berger G (1998) Kaolinite transformation in high molar KOH solutions. Applied Geochemistry. Vol. 13: 619-629.

Breck DW (1974) Zeolite Molecular Sieves: Structure, Chemistry, and Use. John Wiley, New York.

Buhl JC (1991) Synthesis and characterization of the basic and non-basic members of the cancrinite-natrodavyne family. Thermochimica Acta. Vol. 178: 19-31.

Buhl JC, Loens J (1996) Synthesis and crystal structure of nitrate enclathrated sodalite $Na_8[AlSiO_4]_6(NO_3)_2$. Journal of Alloys and Compounds. Vol. 235: 41-47.

Buhl, JC, Stief, F, Fechtelkord, M, Gesing, TM, Taphorn, U, Taake, C (2000a) Synthesis, X-ray diffraction and MAS NMR characteristics of nitrate cancrinite $Na_{7.6}[AlSiO_4]_6(NO_3)_{1.6}(H_2O)_2$. Journal of Alloys and Compounds. Vol. 305: 93-102.

Buhl, JC, Hoffmann, W, Buckermann, WA, Muller-Warmuth, W (2000b) The crystallization kinetics of sodalites grown by the hydrothermal transformation of kaolinite studied by 29Si MAS NMR. Solid State Nuclear Magnetic Resonance. Vol. 9: 121-128.

Chorover J, Choi S, Amistadi M, Karthikeyan K, Crosson G, Mueller K (2003) Linking Cesium and Strontium uptake to kaolinite weathering in simulated tank waste leachate. Environmental Science & Technology. Vol. 37: 2200-2208.

Choi, S, Amistadi, MK, Chorover, J (2005a) Clay mineral weathering and contaminant dynamics in a caustic aqueous system I. Wet chemistry and aging effects. Geochimica et Cosmochimica Acta. Vol. 69, No. 18: 4425-4436.

Choi, S, Crosson, G, Mueller, KT, Seraphin, S, Chorover, J (2005b) Clay mineral weathering and contaminant dynamics in a caustic aqueous system II. Mineral transformation and microscale partitioning. Geochimica et Cosmochimica Acta. Vol. 69, No. 18: 4437-4451.

Coombs, DS, Alberti, A, Armbruster, T, Artioli, G, Colella, C, Galli, E (1997) Recommended nomenclature for zeolite minerals: Report of the subcommittee on zeolites for the International Mineralogical Association, Commission on New Minerals and Mineral Names. The Canadian Mineralogist. Vol. 35: 1571-1606.
Covarrubias C, García R, Arriagada R, Yanez J, Garland T (2006) Cr(III) exchange on zeolites obtained from kaolin and natural mordenite. Microporous and Mesoporous Materiales. Vol. 88: 220-231.
Deng, Y, Harsh, JB, Flury, M, Young, J, Boyle, J (2003) Mineral phase transformation in conditions mimic sediment solutions underlying leaked Hanford waste tanks. Abstracts, The Clay Minerals Society 40th Annual Meeting: June 7-12, Athens, Georgia, pp. 50-51.
Dudzik Z, Kowalak S (1974) Preparation of zeolites of faujasite type from kaolinite. Przemys´l Chemiczny. Vol. 53: 616 -618.
Flury M, Mathison J, Harsh J (2002) In situ mobilization of colloids and transport of cesium in Handford sediments. Environmental Science & Technology. Vol. 36: 5335-5341.
Gerson, AR, Zheng, K (1997) Bayer process plant scale: transformation of sodalite to cancrinite. Journal of Crystal Growth. Vol. 171: 209-218.
Gualtieri, A, Norby, P, Artioli, G, Hanson, J (1997) Kinetic study of hydroxysodalite formation from natural kaolinites by time-resolved synchrotron powder diffraction. Microporous Materials. Vol. 9: 189-201.
Lobo, RF, Zones, SI, Davis, ME (1995) Structure-direction in zeolite synthesis. Journal of Inclusion Phenomena and Macrocyclic Chemistry. Vol. 21: 47-78.
Mashal, KY (2003) Characterization of colloids from Hanford formation sediments reacted with simulated tank waste. Unpublished PhD thesis, Washington State University, 135p.
Mon J, Deng Y, Flury M, Harsh J (2005) Cesium incorporation and diffusion in cancrinite, sodalite, zeolite,and allophane. Microporous and Mesoporous Materiales. Vol. 86: 277-286.
Park M, Choi C, Lim W, Kim M, Choi J, Heo N (2000) Molten-salt method for the synthesis of zeolitic materiales: I. Zeolite formation in alkaline molten-salt system. Microporous Mesoporous Materiales. Vol. 37: 81-89.
Rees L, Chandrasekhar S (1993) Hydrothermal reaction of kaolinite in presence of fluoride ions at pH less than 10. Zeolites. Vol. 13: 534-541.
Serne R, Zachara J, Burke D (1998) Chemical information on tank supernatants, Cs adsorption from tank liquids onto Hanford sediments, and field observations of Cs migration from past tank leaks. PNNL-11498/UC-510, Pacific Northwest National Laboratory, Richland, Washington.
Sinha, PK, Paniker, PK, Amalraj, RV (1995) Treatment of radioactive liquid waste containing caesium by indigenously available synthetic zeolites: a comparative study. Waste Management. Vol. 15: 149-157.
Valcke, E, Engels, B, Cremers, A (1997) The use of zeolites as amendments in radiocaesium- and radiostrontium-contaminated soils: A soil-chemical approach. Part II.: Sr-Ca exchange in clinoptilolite, mordenite and zeolite A. Zeolites. Vol. 18: 212-217.
Zhao H, Deng Y, Harsh J, Flury M, Boyle J (2004) Alteration of Kaolinite to Cancrinite and Sodalite by Simulated Hanford Tank Waste and its impact on Cesium retention. Clays and Clay Minerals. Vol. 52, No. 1: 1-13.